

1 **On the Holocene Evolution of the Ayeyawady Megadelta**

2
3 Authors:

4
5 Liviu Giosan¹, Thet Naing², Myo Min Tun³, Peter D. Clift⁴, Florin Filip⁵,
6 Stefan Constantinescu⁶, Nitesh Khonde^{1,7}, Jerzy Blusztajn¹, Jan-Pieter Buylaert⁸,
7 Thomas Stevens⁹, Swe Thwin¹⁰

8
9 Affiliations:

10
11 ¹Geology & Geophysics, Woods Hole Oceanographic, Woods Hole, USA

12 ²Patheingyi University, Patheingyi, Myanmar

13 ³University of Mandalay, Mandalay, Myanmar

14 ⁴Geology & Geophysics, Louisiana State University, USA

15 ⁵The Institute for Fluvial and Marine Systems, Bucharest, Romania

16 ⁶Geography Department, Bucharest University, Bucharest, Romania

17 ⁷Birbal Sahni Institute of Palaeosciences, Lucknow, India

18 ⁸Technical University of Denmark, Roskilde, Denmark

19 ⁹Uppsala University, Uppsala, Sweden

20 ¹⁰Mawlamyine University, Mawlamyine, Myanmar

21
22
23
24
25
26 Correspondence to: L. Giosan (lgiosan@whoi.edu)

37 Abstract:

38

39 The Ayeyawady delta is the last Asian megadelta whose evolution has remained
40 essentially unexplored so far. Unlike most other deltas across the world, the Ayeyawady
41 has not yet been affected by dam construction providing a unique view on largely natural
42 deltaic processes benefiting from abundant sediment loads affected by tectonics and
43 monsoon hydroclimate. To alleviate the information gap and provide a baseline for future
44 work, here we provide a first model for the Holocene development of this megadelta
45 based on radiocarbon and optically stimulated luminescence-dated trench and drill core
46 sediments collected in 2016 and 2017, together with a re-evaluation of published maps,
47 charts and scientific literature. Altogether, this data indicates that Ayeyawady is a mud-
48 dominated delta with tidal and wave influences. The sediment-rich Ayeyawady River
49 built meander belt alluvial ridges with avulsive characters. A more advanced coast in the
50 western half of delta (i.e., the Pathein lobe) was probably favored by the more western
51 location of the early course of the river. Radiogenic isotopic fingerprinting of the
52 sediment suggest that the Pathein lobe coast does not receive significant sediment from
53 neighboring rivers. However, the eastern region of the delta (i.e., Yangon lobe) is offset
54 inland and extends east into the mudflats of the Sittaung estuary. Wave-built beach ridge
55 construction during the late Holocene, similar to other several deltas across the Indian
56 monsoon domain, suggests a common climatic control on monsoonal delta
57 morphodynamics through variability in discharge, changes in wave climate, or both.
58 Correlation of the delta morphological and stratigraphic architecture information onland
59 with the shelf bathymetry, as well as its tectonic, sedimentary and hydrodynamic
60 characteristics provide insight on the peculiar growth style of the Ayeyawady delta. The
61 offset between the western Pathein lobe and the eastern deltaic coast appears to be driven
62 by tectonic-hydrodynamic feedbacks as the extensionally lowered shelf block of the Gulf
63 of Mottama amplifies tidal currents relative to the western part of the shelf. This situation
64 probably activates a perennial shear front between the two regions that acts as a leaky
65 energy fence. Just as importantly, the strong currents in the Gulf of Mottama act as an
66 offshore-directed tidal pump that help build the deep mid-shelf Mottama clinof orm with
67 mixed sediments from Ayeyawady, Sittaung, and Thanlwin rivers. The highly energetic
68 tidal, wind and wave regime of the northern Andaman Sea thus exports most sediment
69 offshore despite the large load of the Ayeyawady river.

70

71 Introduction

72

73 Asian megadeltas (*Woodroffe et al., 2006*) have a long history of human habitation and
74 anthropogenic impact. With large populations, which increasingly congregate in
75 sprawling megacities, these vast low-lying and ecologically-rich regions are under threat
76 from environmental degradation, climate change and sea level rise. The Ayeyawady
77 (formerly known as Irrawaddy or Ayeyarwady) is the least studied of these megadeltas
78 despite its scientific, social and economic importance (*Hedley et al., 2010*). Located in
79 the larger India-Asia collision zone, the Ayeyawady delta (Fig. 1) bears the imprint of
80 uniquely complex tectonic processes in a region of oblique subduction (*Morley et al.,*
81 *2017*) and is a repository for unusually large sediment yields under an erosion-prone
82 monsoon climate (e.g., *Giosan et al., 2017*). Sediment redistribution within the delta and
83 on the shelf fronting it is affected by strong tides amplified by the geomorphology of the
84 region (*Ramasawamy and Rao, 2014*). In contrast to other Asian megadeltas, the
85 Ayeyawady river basin is arguably less transformed by post-World War II anthropogenic
86 impacts although humans have probably affected delta development since at least the Iron
87 Age as agriculture expanded along the river (*Moore, 2007*) and later intensified during
88 the Pyu (~200 BC to 1050 AD), Bagan (~850 to 1300 AD), and Ava (~1350 to 1550 AD)
89 historical periods. Recent rapid development trends and population growth underline the
90 need to understand the history and document the current state of the Ayeyawady delta.

91

92 Although the Ayeyawady River is less regulated compared to other large rivers, plans are
93 afoot to construct several dams across it and this may change the water and sediment
94 regimes, as well as fluxes reaching its low-lying delta plain (*Brakenridge et al., 2017*).
95 Inundation of the Ayeyawady delta region during cyclone Nargis in 2008 was one of the
96 costliest and deadliest natural disasters ever recorded (*Fritz et al., 2009; Seekins, 2009*).
97 Catastrophic monsoon-driven river floods are also common and devastating (*Brakenridge*
98 *et al., 2017*). The Ayeyawady delta may already be sediment deficient (*Hedley et al.,*
99 *2010*) and the anticipated sediment deficit after damming could increase its vulnerability
100 to such transient events as well as to long term sea level rise (*Giosan et al., 2014*). Strong
101 tidal currents in the northern Andaman Sea (*Rizal et al., 2012*) amplify some aspects of
102 delta vulnerability, such as salinization (*Taft and Evers, 2016*) whereas other aspects may
103 be attenuated such as sediment redistribution along the coast or sediment trapping within
104 the subaerial delta (e.g., *Hoitink et al., 2017*). Better knowledge on how the delta has
105 formed and functioned will help future efforts to maintain it viable.

106

107 To alleviate the information gap and provide a baseline for future work we sketch here a
108 first model for the Holocene evolution of the Ayeyawady delta based on new field data
109 collected in two expeditions in 2016 and 2017 (Figs. 2 and 3; see Fig. S1 for site
110 locations and names) together with a re-evaluation of published maps, charts and
111 scientific literature (Fig. 4 and 5). In the process we reassess our knowledge concerning

112 monsoonal deltas in general by advancing new ideas on how morphodynamics and
113 sedimentary architecture can be controlled by feedbacks between tectonics and tides as
114 well as by the balance between fluvial discharge and wave climate.

115

116 Background

117

118 The Ayeyawady River is a major fluvial system that became individualized in
119 Oligocene/Early Miocene time (Fig. 1; *Licht et al., 2016; Morley, 2017* and references
120 therein). The upper Cretaceous subduction of the Neotethys Ocean followed by the
121 collision between India and Asia first led to an Andean-type margin comprised of the
122 Wuntho-Popa Volcanic Arc and associated forearc and backarc basins (e.g., *Racey and*
123 *Ridd, 2015; Liu et al., 2016*). The uplift of the Indo-Burman Ranges accretionary prism
124 since early Paleogene completed the separation of the Central Myanmar Basin (CMB)
125 from the Bay of Bengal. The complex of basins forming the CMB were further
126 segmented by compression and inversion (e.g., *Bender, 1983*). These basins include the
127 Ayeyawady Valley separated by the Bago Yoma (Pegu Yoma) from the Sittaung
128 (Sittang) Valley flowing along the Shan Plateau. The Ayeyawady River infilled this ~900
129 km long shallow marine area toward the Andaman Sea, a Cenozoic backarc/strike-slip
130 basin induced by oblique subduction of the Indian plate under Eurasia (e.g., *Curry,*
131 *2005*). A southern shift in Ayeyawady deposition was evident in the Miocene after the
132 strike-slip Sagaing Fault activated along Bago Yoma. The Holocene delta is the last
133 realization in a series of deltas comprising this southward-moving Ayeyawady
134 depocenter.

135

136 Myanmar's hydroclimate that is responsible for Ayeyawady flow is spatially complex
137 owing to its varied topography and compound influences from both the Indian and East
138 Asian monsoon systems (*Brakenridge et al., 2017*). Orographic precipitation occurs
139 along the northeastern Himalayas and Indo-Burman Ranges (*Xie et al., 2006*), as well as
140 the Shan Plateau feeding the upper Ayeyawady and the Chindwin, whereas Central
141 Myanmar, in the lee of these ranges, remains drier. The upper basin of the Ayeyawady
142 also receives snow and glacier meltwater in the spring. Over 90% of the discharge at the
143 delta occurs between May and October with small but significant interannual variability
144 (*Furuichi et al., 2009*) linked to the El Niño-Southern Oscillation, Indian Ocean Dipole,
145 and Pacific Decadal Oscillation (*D'Arigo and Ummenhofer, 2014* and references therein).

146

147 In historical times the Ayeyawady River has transported $\sim 422 \pm 41 \times 10^9 \text{ m}^3$ of
148 freshwater every year to the ocean (*Robinson et al, 2007*), watering Myanmar from north
149 to south along the way (Fig. 1). The water discharge apparently decreased to the present
150 level of $379 \pm 47 \times 10^9 \text{ m}^3/\text{year}$ (*Furuichi et al., 2009*). Among the delta-building
151 Himalayan rivers, the Ayeyawady is a prodigious sediment conveyor ($\sim 364 \pm 60 \times 10^6$

152 t/year), second only to the combined Ganges-Brahmaputra (*Robinson et al., 2007*).
153 Between 40 and 50 % of the sediment comes from the upper Ayeyawady with the rest
154 supplied by its main tributary, the Chindwin (*Garzanti et al., 2016*). Sediments
155 transported by the Upper Ayeyawady River come primarily from erosion of gneisses and
156 granitoids of the Himalayan Eastern Syntaxis region and the Sino-Burman Ranges.
157 Although draining less steep terrain, the Chindwin contributes more sediment than the
158 Upper Ayeyawady from the easily erodible flysch and low-grade metasedimentary rocks
159 of the Indo-Burman Ranges. Both water and sediment discharge vary synchronously at
160 interannual time scales as a function of monsoon intensity (*Furuichi et al., 2009*), but
161 they changed little since the late 19th century when *Gordon (1893)* measured them
162 systematically for the first time. In addition to the Ayeyawady, the Sittaung River
163 supplies sediment to the northern shore of the Gulf of Mottama (*aka* Gulf of Martaban)
164 where its estuary merges with the Ayeyawady delta coast (Fig. 1). The sediment
165 discharge from the Sittaung is unknown but can be estimated based on its annual water
166 discharge range from $50 \times 10^9 \text{ m}^3$ to a maximum of 40 to $50 \times 10^6 \text{ t/year}$ by assuming
167 sediment yields similar to the Ayeyawady's (*Milliman and Farnsworth, 2010*). Another
168 sediment contributor to the Gulf of Mottama ($\sim 180 \times 10^6 \text{ t/year}$; *Robinson et al., 2007*) is
169 the Thanlwin River (Salween) draining the eastern Shan Plateau and eastern Tibetan
170 Plateau. Information about the variability in Ayeyawady's sediment discharge over the
171 Holocene lifetime of the delta is sparse, as are reconstructions for the monsoon regime in
172 its basin. Assuming the modern direct correlation between water discharge and sediment
173 load one may qualitatively infer an increase in sediment delivery since 10,000 years ago
174 with a peak in around 5000 years ago when the Andaman Sea was at its freshest
175 (*Gebregeorgis et al., 2016*), followed by a decrease to the present values, as the Indian
176 monsoon has weakened since the Early Holocene (e.g., *Ponton et al., 2012*).

177
178 The Ayeyawady delta is a mud-dominated delta that exhibits mainly tidal and secondarily
179 wave influences (Figs. 2 and 5; *Kravtsova et al., 2009*). Ayeyawady's single braided
180 channel starts to show avulsive behaviour near the town of Myan Aung ($\sim 18.2^\circ \text{N}$) where
181 the tidal influence is still felt $\sim 290 \text{ km}$ from the Andaman Sea (Fig. 1). The apex of the
182 delta, defined as the region of deltaic distributary bifurcation, is north of the town of
183 Hinthada (18°N) around 270 km from the coast. Multiple branches are active in the delta,
184 splitting and rejoining to form a network of higher order distributary channels and
185 reaching the coast through eleven tidally-enlarged estuaries (Fig. 2). Most of the water
186 discharge (76%) is delivered to the Andaman Sea through three main mouths: Pyamalaw,
187 Ayeyawady and To-Thakutpin from west to east (*Kravtsova et al., 2009*).

188
189 In natural conditions when the delta was covered by tropical forests and mangroves
190 (*Adas, 2011*), sedimentation on the delta plain occurred within active and abandoned
191 channels, on channel levees and inter-distributary basins (*Stamp, 1940; Kravtsova et al.,*

192 2009). The coast prograded via shoal/bar emergence and wave-built beach ridges with
193 associated interridge swales (*Kravtsova et al., 2009*). The coastline for the Ayeyawady
194 delta proper stretches from the western rocky Cape Maw Deng (formerly Pagoda Point),
195 adjacent to the Patheingyi River, to the Yangon River in the east (Fig. 1). However, this
196 conventional definition does not capture the fact that the accumulative coast with
197 sediment input from the Ayeyawady continues east of Yangon River into the Sittaung
198 estuary. Despite the large fluvial sediment load of the combined Ayeyawady and Sittaung
199 delivered annually ($350\text{--}480 \times 10^6$ t), shoreline changes have been puzzlingly minor
200 along the Ayeyawady delta coast since 1850 (*Hedley et al., 2010*). Sea level change data
201 is sparse and unreliable for the delta and no data on subsidence/uplift exists.
202

203 The shelf morphology in front of the Ayeyawady delta is complex due to its tectonic
204 structure and the nature of Holocene sedimentation (*Rodolfo, 1969a,b, 1975*;
205 *Ramaswamy and Rao, 2014*). The width of the shelf is ~170 km wide off the Ayeyawady
206 River mouths, widening to more than 250 km in the Gulf of Mottama (Figs. 1 and 5). The
207 shelf edge exhibits a flat, platform-like indentation in the Gulf of Mottama between 140
208 and 180 m deep (i.e., the Martaban Depression - *Ramaswamy and Rao, 2014*) that
209 features a dendritic network of channels feeding the Martaban Canyon (*Rodolfo, 1975*).
210 Most of the large Ayeyawady sediment suspended load is redistributed by the strong tidal
211 currents (Fig. 5) and seasonally-reversing wind-currents to be deposited on the wide
212 northern Andaman shelf (*Ramaswamy and Rao, 2014*) where it mixes with sediment
213 from the Sittaung, Thanlwin and other smaller rivers (*Damodararao et al., 2016*). Semi-
214 diurnal tides vary between 2 and 3 m from the Patheingyi River to the Bogale River reaching
215 higher stages inside distributaries. The tidal range is gradually amplified to macrotidal
216 conditions on the shallow (<30 m) shelf of the Gulf of Mottama from the Bogale
217 Promontory toward the Sittaung estuary where it reaches above 7 m during spring tides
218 (*British Admiralty, 1935*). Associated tidal currents also vary accordingly to over 3.5 m/s
219 near the Sittaung mouth.
220

221 Waves are subordinate in importance to tides, with average heights less than 1 m in
222 winter to 1–2 m in summer (*Kravtsova et al., 2009*). Tidal currents combine with the
223 wind-driven circulation. Wind currents are clockwise during the summer monsoon and
224 reversed during the winter monsoon (*Rizal et al., 2012*). The macrotidal regime maintains
225 turbid conditions year-round with the turbidity front oscillating ~150 km in the Gulf of
226 Mottama in phase with the spring-neap tidal cycle (*Ramaswamy et al. 2004*). Annual
227 turbidity levels and suspended sediment distribution are modulated by the monsoonal-
228 driven winds, currents and river discharge (*Ramaswamy et al. 2004; Matamin et al,*
229 *2015*) with the most extensive and compact turbid waters occurring in boreal winter.
230 During the summer the turbidity region shrinks to the Gulf of Mottama and nearshore
231 regions where river plumes are active and dispersed eastward. Turbidity profiles show an

232 increase with depth during fair-weather and uniform concentrations during major storms
233 or cyclones (*Ramaswamy et al. 2004; Shi and Wang 2008*). Bottom nepheloid layers and
234 possibly hyperpycnal flows occur in the Gulf of Mottama and flow into the interior of the
235 Andaman Sea as mid-water nepheloid layers (*Ramaswamy et al., 2004*).

236

237 The bathymetric characteristics of the shelf and the circulation system favor deposition of
238 fine fluvial sediments in a mudbelt that widens from western edge of the Ayeyawady
239 coast into the Gulf of Mottama that more or less coincides in extent with the high
240 turbidity region (*Ramaswamy and Rao, 2014*). The outer shelf, including the Martaban
241 Depression, is a zone of low to non-deposition, and exhibits a relict morphology with
242 topographic irregularities that host relict coarse-grained carbonate-rich sediment and
243 fauna with patchy Holocene muds (*Ramaswamy and Rao, 2014*).

244

245 In terms of human impacts on the delta it is important to note that the population of
246 Myanmar increased from 4–5 million in the late 19th century to ~51 million in 2014 with
247 30% residing in the Ayeyawady delta region. This large increase in population led to a
248 rapid rate of deforestation in the basin, but also to destruction of mangroves for
249 agriculture and fuel in the delta (*Taft and Evers, 2016*). An earlier large migration wave
250 to the delta occurred in the latter half of the 19th century when the British colonial
251 authorities cleared much of the delta forests and mangroves for rice agriculture (*Adas,*
252 *2011*). Construction of dikes to protect agricultural lands in the delta began in 1861 and
253 continued aggressively until the 1920s. These dikes are generally of a horseshoe type
254 protecting delta islands in the upstream and sides from the floodwave but recently
255 poldering with diking entire islands was employed. Most channels remain natural with no
256 extensive system of dredged canals. However, all dikes limit overbank flooding and
257 deposition of sediment (*Volker 1966; Stamp 1940*) and the entire agricultural system
258 favors salinization of soils in the delta. The model for the Holocene evolution of the
259 Ayeyawady delta that we provide below allows us to assess first order relationships to the
260 complex regional tectonics, climate, and shelf circulation as a baseline for the future
261 development and management of the delta.

262

263 Methods

264

265 The large scale morphology of the Ayeyawady delta, together with the adjoining regions
266 (Fig. 2), were assessed and studied using satellite data and old maps of the region. High-
267 resolution (90-m) digital elevation data were derived from NASA's Shuttle Radar
268 Topography Mission (SRTM; *Farr et al., 2007*). Digital elevation models (DEMs) were
269 constructed at 300 m resolution and were used in combination with Advanced
270 Spaceborne Thermal Emission and Reflection Radiometer (ASTER) and Google Earth to
271 identify geomorphic features that provide insight into fluvial morphodynamics. The delta
272 and upstream floodplain was delimited from adjacent hinterlands with associated

273 marginal alluvial fans as were remnant inselberg-like pre-deltaic terrains inside the delta.
274 We identified active and abandoned river courses and delta distributaries and their
275 meander belts. Finally, we identified fossil beach ridges denoting former delta shorelines.
276 Guided by this assessment, in two field expeditions in the Ayeyawady delta in 2016 and
277 2017, we collected sedimentary records from shallow hand-dug trenches and cores with
278 mechanized pneumatic and percussion drilling (Figs. 2 and 3; see also Fig. S1).

279
280 Fossil wave-built beach ridges were targeted by trenching in order to obtain a chronology
281 for the delta coast advance (Figs. 1 and 2; see also Fig. S1). Samples for Optically
282 Stimulated Luminescence (OSL) dating were collected where possible from within the
283 beach-foreshore facies in water tight opaque tubes (site I-11 at Labutta in the western side
284 of the delta; sites I-12 and I-13 at Seikma near the central delta coast; and site I-14 at
285 Kungyangan near the eastern delta coast). A sample was collected in the anthropogenic
286 overburden to date habitation on a Labutta beach ridge (Site I-10). In addition, two levee
287 samples were collected on meanders of the now defunct western major branch of the
288 Ayeyawady (Figs. 1 and 2; Table 2) near the apex of the delta (i.e., sites I-8 near Ta Loke
289 Htaw and I-9 near Lemyethna bordering the last abandoned course and an earlier-formed
290 oxbow lake, respectively). Levee samples were collected in trenches at the top of each
291 levee, below the overburden.

292
293 Drill coring was designed to recover continuous sediment records to the pre-deltaic
294 Pleistocene sediments (Figs. 2 and 3; see also Fig. S1; Table 1). Drill sites were located
295 in the middle and near the apex of the delta (core IR1 to 70.4 m depth at Kyonmangay
296 located 6.7 m above sea level and core IR2 to 43 m depth at Ta Loke Htaw located at 18
297 m above sea level, respectively) to assess the deltaic architecture and, in particular, how
298 far the post-glacial transgression reached inside the suspected Pleistocene Ayeyawady
299 incised valley. Facies analysis was based on the visual description of lithology,
300 sedimentary structures, textures and benthic foraminifera presence. In addition, XRF-
301 scanning high resolution chemostratigraphy was employed for the drill cores to identify
302 depositional environments using Woods Hole Oceanographic Institution's (WHOI)
303 ITRAX XRF scanner (see methodology in *Croudace et al., 2006*). From the suite of
304 measured elements we used [Si]/[Rb] ratio to characterize the sand content (i.e., Si-rich
305 sand relative to fine grained muds, rich in Rb; *Croudace and Rothwell, 2015*), the
306 [Br]/[total XRF counts] ratio or Br* to characterize the organic matter (i.e., with Br
307 enriched in marine organic matter; *McHugh et al., 2008*), and [S]/[Rb] ratio to
308 characterize redox conditions in fine-grained muds (i.e., with S in excess of terrigenous
309 values in reducing conditions; *Croudace and Rothwell, 2015*).

310
311 Sediment sources for the pre-modern delta were estimated using radiogenic isotopes (Nd
312 and Sr) on a bulk sediment sample from the delta apex trench (I-8 taken as representative

313 for Ayeyawady fluvial sediment). To assess any potential addition of non-Ayeyawady
314 sediment sources (e.g., littoral drift, marine biogenic carbonates) another pre-modern
315 sample from the youngest dated fossil beach ridge trench near the coast (I-12) was
316 measured both as bulk and decarbonated. The radiogenic composition of sediments from
317 Sittaung River, the closest source to the delta other than Ayeyawady itself, was measured
318 on floodplain sample near Bago (Fig. 1). Nd and Sr chemistry was undertaken with
319 conventional ion chromatography following the method of *Bayon et al. (2002)*. Strontium
320 was separated and purified from samples using Sr-Spec (Eichrom) resin. Nd chemistry
321 was performed with LN resin (Eichrom) following method described in *Scher and*
322 *Delaney (2010)*. Sr and Nd analyses were conducted on the NEPTUNE multi-collector
323 ICP-MS at WHOI with the internal precision around 10–20 ppm (2σ); external precision,
324 after adjusting $^{87}\text{Sr}/^{86}\text{Sr}$ and $^{143}\text{Nd}/^{144}\text{Nd}$ values by 0.710240 and 0.511847 for the
325 SRM987 and La Jolla Nd standards respectively, is estimated to be 15–25 ppm
326 (2σ). $^{143}\text{Nd}/^{144}\text{Nd}$ isotopic composition is expressed further as ϵNd (*DePaolo and*
327 *Wasserburg, 1976*) units relative to $(^{143}\text{Nd}/^{144}\text{Nd})_{\text{CHUR}} = 0.512638$ (*Hamilton et al.,*
328 *1983*).

329

330 Plant and wood pieces were radiocarbon-dated to derive a chronology for the deltaic
331 sediment succession and the pre-deltaic base (Table 1). Accelerator mass spectrometry
332 (AMS) radiocarbon dating was performed at the National Ocean Sciences Accelerator
333 Mass Spectrometry Facility (NOSAMS) at the WHOI. The methodology for AMS
334 radiocarbon dating is presented on the NOSAMS site (www.whoi.edu/nosams) and
335 discussed in *McNichol et al. (1995)*. All dates have been converted to calendar ages using
336 CalPal 4.3 (*Bronk Ramsey, 2009*) and the IntCal13 calibration dataset (*Reimer et al.,*
337 *2013*).

338

339 Seven samples were collected for OSL dating. Samples were collected using light-tight
340 metal tubes hammered horizontally into cleaned sediment surfaces. The tubes were
341 opened under subdued orange light at the Nordic Laboratory for Luminescence Dating
342 (Aarhus University) located at Risø (DTU Nutech) in Denmark. Using standard sample
343 preparation techniques (wet sieving, acid treatment, heavy liquids) purified quartz and K-
344 feldspar-rich extracts in the 180-250 μm grain size range were obtained (except sample
345 177202 for which it was 90-180 μm). Multi-grain aliquots of quartz and K-feldspar were
346 measured using a SAR protocol (*Murray and Wintle, 2000*) suitable for young samples.
347 The purity of the quartz OSL signal was confirmed using OSL IR depletion ratio test
348 (*Duller, 2003*; all aliquots within 10% of unity). For quartz OSL preheating for dose and
349 test dose was 200°C/10s and 160°C, respectively and K-feldspar rich extracts were
350 measured using a post-infrared (IR) Infrared Stimulated Luminescence (IRSL)
351 (pIRIR150) protocol based on *Madsen et al. (2011)*. Early and late background
352 subtraction was used for quartz OSL and feldspar pIRIR dose calculations respectively.

353 Total dose rates to quartz and K-feldspar were calculated from radionuclide
354 concentrations measured on the outer material from the tubes using high resolution
355 gamma ray spectrometry (Murray *et al.*, 1987). Samples were assumed to have been
356 saturated with water throughout the entire burial lifetime.

357
358 The morphology of the subaqueous extension of the Ayeyawady delta was studied using
359 the only available detailed bathymetric chart of the region that was based on surveys from
360 1850 to 1929 with small corrections until 1935 (*British Admiralty, 1935*). Newer
361 navigation charts of the region report only small corrections afterwards. The final DEM
362 (Figs. 4 and 5) consists of 6442 individual soundings reduced to the original datum at
363 Elephant Point at the entrance in Yangon River; to these we added the digitized
364 bathymetric contours of the original chart. To extend the bathymetry offshore beyond the
365 coverage of the original chart we used GEBCO 2014 Grid (General Bathymetric Charts
366 of the Oceans, a global 30 arc-second interval grid). Prior to digitizing, all charts and
367 satellite photos used in this study were georeferenced and transformed to a common
368 UTM projection (Zone 46 N) with Global Mapper 18.0 ([http:// www.globalmapper.com/](http://www.globalmapper.com/))
369 using 16 control points for each chart or photo. DEMs at a 250 m spatial resolution were
370 generated from digitized soundings with Surfer 12.0 software (Golden Software, Inc.).
371 The “natural neighbor” algorithm was chosen for interpolation because it is suitable for
372 a variable density of data across the interpolation domain and does not extrapolate depth
373 values beyond the range of existing data.

374 375 Results

376
377 In concert with satellite photos, our SRTM digital elevation model (Fig. 2a) reveals that
378 the morphologically-defined Ayeyawady delta plain starts immediately after the river
379 emerges from its mountainous valley at Myan Aung, bound on the western side by the
380 Indo-Burma Range and massive alluvial fans originating in the Bago Yoma on the
381 eastern side. Several inselberg-like pre-deltaic high terrains occur close to the coast on
382 the western side of Patheingyi River and on both sides of Yangon River. Two alluvial ridges,
383 5 to 7 m high relative to their adjacent delta plain, with visible meander belts and rare
384 crevasse splays, were constructed by large trunk channels (Fig. 2a, b, c). The western
385 alluvial ridge along the Daga course is largely fossil, whereas the eastern ridge is being
386 built along the present course of the river (Fig. 2c). Both ridges taper off in the mid-delta
387 as the trunk channels start to bifurcate into distributaries that split and rejoin on the lower
388 delta (Fig. 2a,b). After the bifurcation zone the delta plain is uniformly low in altitude (<5
389 m) with the exception of the higher mudflats near the entrance in the Sittaung estuary
390 (Fig. 2a). Although possessing meander belts of their own in their upper reaches, the
391 Patheingyi and Yangon Rivers, located at the western and eastern edge of the delta, do not
392 show visibly large alluvial ridges (Fig. 2a, b) suggesting that they were not preferential
393 routes for the main trunk Ayeyawady but secondary courses or have not been active for

394 very long. Near the coast, several generations of wave-built beach ridges are evident in
395 the lower part of the delta, bundling occasionally into beach ridge plains on the Bogale
396 Promontory and on the sides on Yangon River (Fig. 2b).
397

398 Sediment in our trenches on the Ayeyawady beach ridges exhibited weakly stratified,
399 mud-rich, fine sand lithologies. Fluvial deposits trenched near the apex showed a typical
400 levee facies exhibiting weakly laminated, amalgamated fine sands and muds below the
401 bioturbated and human-disturbed overburden. The IR1 drill core (Fig. 3) at Kyonmangay
402 (Fig. 2; see also Fig. S1) shows a succession of delta plain bioturbated soils and delta
403 plain muds overlaying amalgamated fine to medium sand and muds of the delta front and
404 prodelta/estuarine clayey muds with intercalated organic-rich detritus layers. Marine
405 influences are documented in the prodelta/estuarine and delta front deposits by high Br*
406 and rare benthic foraminifers. Tidal influence is indicated by thick-thin and sand-mud
407 alternations in the delta front deposits. Flooding is suggested by occasional clean sandy
408 layers in the prodelta facies. Both the delta plain and prodelta/estuarine deposits show
409 increased S/Rb values indicating poorly oxic conditions. The transition to delta front
410 advance at Kyonmangay occurred at 13.5 m below sea level (mbsl) ~8,100 years ago, as
411 documented by the radiocarbon content of a leaf fragment. The deltaic succession stands
412 on a 9,300 years old mangrove peat at 28.5 mbsl near the base of the deltaic Holocene
413 deposits. Pre-Holocene fluvial deposits older than 10,200 years BP occur below,
414 consisting of structureless medium to coarse sands with clayey mud intercalations,
415 gravels, and fine-grained weakly laminated channel infills.
416

417 The IR2 drill core (Fig. 3) at Ta Loke Htaw (Fig. 2; see also Fig. S1) near the delta apex
418 on the modern alluvial ridge exhibits a succession of delta plain sandy muds topping
419 structureless medium sands with rare intercalated thin muds of channel/point bar type.
420 They overlie fine-grained, weakly laminated channel infill deposits and floodplain fine
421 sands with intercalated thin muds that started to accumulate ~8,900 years BP
422 (radiocarbon dated wood piece). Below ~25 mbsl structureless fine to medium sands of
423 channel/point bar and gravel layers occur to the base of the drill core. Organic material is
424 rare in all facies at Ta Loke Htaw except for occasional wood branches and a tree trunk in
425 the upper point bar facies. Marine influence is absent as foraminifers are not encountered
426 and Br* levels are consistently low.
427

428 The quartz OSL and feldspar pIRIR150 luminescence dating results are summarized in
429 Table 2 and Table S1. The quartz OSL signal is dominated by the fast component and the
430 average dose recovery ratio is 1.00 ± 0.02 (4 samples, 11-12 aliquots per sample)
431 suggesting that our quartz De values measured using SAR are reliable. One prerequisite
432 for accurate age estimation is that the quartz OSL signal was sufficiently bleached prior
433 to burial in the sediment sequence. In this study we use the feldspar IR50 and pIRIR150

434 age data to provide insights into the completeness of bleaching of the quartz OSL signal
435 (e.g., *Murray et al., 2012; Rémillard et al., 2016*). This is based on the observation that
436 feldspar signals bleach much more slowly than quartz OSL (*Godfrey-Smith et al., 1988;*
437 *Thomsen et al., 2008*): IR50 signals bleach approximately one order of magnitude slower
438 than quartz OSL and pIRIR signals bleach even more slowly than IR50 signals (e.g.,
439 *Kars et al., 2014; Colarossi et al., 2015*). We are confident that the quartz signal is well-
440 bleached when the pIRIR150 age agrees within uncertainty with the quartz age; this is the
441 case for sample 177204. We consider that the quartz OSL signal is very likely to be
442 completely bleached when the IR50 age agrees or is slightly lower (due to fading) than
443 the quartz age. This is the case for all samples except for sample 177202 for which the
444 IR50 age may be slightly older. Nevertheless, this does not mean the quartz OSL age for
445 this particular sample is affected by partial bleaching; we just cannot be certain it is not.

446

447 Overall, optical ages on the natural levee of an oldest meander series of the fossil eastern
448 alluvial ridge indicate full activity by $\sim 1,750 \pm 320$ years ago. Sedimentation on the top of
449 the natural levee bordering the last Daga course indicate that its abandonment took place
450 no earlier than $1,500 \pm 230$ years ago (Fig. 2; see also Fig. S1). A radiocarbon date
451 calibrated to $\sim 1,300$ years ago on a large wood trunk from the point bar facies drilled at
452 Ta Loke Htaw indicates that the present eastern course of the Ayeyawady was active at
453 the time. The fresh appearance of the wood make it unlikely that it is remobilized fossil
454 wood. However, a future systematic exploration of the meander belts subsurface
455 architecture is needed to reconstruct their history.

456

457 Our combined chronology indicates the Ayeyawady delta reached as far south as the
458 latitude of the cities of Yangon and Patheingyi around 6,300 years ago, as documented by a
459 radiocarbon content of a leaf fragment from the delta plain facies at Kyonmangay.

460 Optical dating shows that the least advanced beach ridge bundle found on the western
461 side of the delta near Labutta is also the oldest ($\sim 4,600$ years old; Fig. 2 and Fig. S1). The
462 beach ridge plain at the Bogale Promontory started $\sim 1,000$ years ago, soon after beach
463 ridges started to form at the Yangon River mouth ($\sim 1,200$ years ago; Fig. 2 and Fig. S1).

464

465 Radiogenic provenance fingerprinting of the bulk river sediment (Table S2) on the Ta
466 Loke Htaw levee shows that $^{143}\text{Nd}/^{144}\text{Nd}$ (ϵNd) and $^{87}\text{Sr}/^{86}\text{Sr}$ values of 0.512263 (-7.3)
467 and 0.7120 respectively, close to the beach ridge sediment composition: 0.512285 (-6.9)
468 and 0.7118 for bulk sediment and 0.512287 (-6.8) and 0.7119 for bulk decarbonated
469 sediment. The identical $^{87}\text{Sr}/^{86}\text{Sr}$ values for the bulk and decarbonated beach ridge sample
470 suggest that marine biogenic carbonates are a minor sediment component at the coast.
471 However, previous measurements on Ayeyawady sediments (Table S2 with data from
472 *Allen et al., 2008* – 150 km upstream of the delta; *Colin et al., 1999* – at an unspecified
473 location) show a larger variability in ϵNd with values of -8.3 and -10.7. The closest

474 sediment source along the coast, the Sittaung River that drains Bago Yoma and the Shan
475 Plateau shows $^{143}\text{Nd}/^{144}\text{Nd}$ (ϵNd) and $^{87}\text{Sr}/^{86}\text{Sr}$ values of 0.512105 (-10.4) and 0.7168
476 respectively. Yangon River, the largely abandoned easternmost branch of the Ayeyawady
477 close to Bago Yoma has ϵNd and $^{87}\text{Sr}/^{86}\text{Sr}$ of -12.2 and 0.7080 respectively
478 (*Damodararao et al., 2016*), which suggest mixing with a source similar to Sittaung.

479
480 Our reassessment of the late 19th – early 20th century bathymetry with the high-resolution
481 digital elevation model produced several surprises (Figs. 3 and 4a). First, the edge of the
482 shelf (Fig. 4) was found to be significantly deeper in front of the Mottama Depression
483 (>150 m) then west of it (100–120 m deep). Second, the mud belt along the Ayeyawady
484 delta exhibits a clinoform attached to the shore and likely composed of sandy muds (*Rao*
485 *et al., 2005*) and extending to depths of 35–40 m. In contrast, the Gulf of Mottama
486 exhibits a thick mid-shelf clinoform probably comprised of finer muds (*Rao et al., 2005*)
487 with the steep frontal region extending from 40 to 90 m water depth. The transition
488 between the western and eastern clinoforms is marked by a transversal channel that is 10
489 km wide and 5 m deep on average and is flanked on the deeper eastern side by a drift-like
490 elongated feature of similar average dimensions. Third, a flatter area of the outer shelf in
491 front of the western Ayeyawady delta coast stands out from the typical outer shelf chaotic
492 relief, suggesting potential preservation of a relict pre-Holocene delta region at water
493 depths between 35 and 45 m.

494 Discussion

495
496
497 Our new drill core information (Fig. 3) indicate that the Ayeyawady delta advanced into
498 an incised valley estuarine embayment that extended north of Kyonmangay (~80 km
499 from the current coast) but did not reach as far as the current delta apex at Ta Loke Htaw
500 (270 km from the coast). The Pleistocene deposits of the incised valley intercepted in our
501 cores are fluvial, generally much coarser than the delta deposits but heterolithic with
502 indications of increasing tidal influence nearer to the Andaman Sea at Kyonmangay. The
503 overlying peats atop mudflat sediments sampled at Kyonmangay indicate the presence of
504 a muddy coast with mangroves at the time of their transgression ~9,300 years ago. Given
505 that the contemporaneous ice-volume equivalent global sea level was between -29 and -
506 31 mbsl (*Lambeck et al., 2014*), the altitude of the mangrove peat (-28.3 mbsl) on the
507 largely incompressible Pleistocene deposits below indicate that the delta is vertically
508 stable. However, glacial isostatic adjustment modeling is needed to quantify subsidence
509 as neighboring regions of Thailand and Malay Peninsula (*Bradley et al., 2016*) suggests
510 that relative sea level reached higher earlier during the deglaciation. After the mangrove
511 coast was flooded, the marine embayment accumulated estuarine/prodelta muds
512 afterwards. At 8,100 years ago the Ayeyawady bayhead delta front reached the southern
513 Kyonmangay site and by ~6,300 years ago delta plain deposition started.

514

515 Deposits at the delta apex in the drill core at Ta Loke Htaw indicate a dynamic fluvial
516 environment with channel erosion (i.e., scouring) followed point bar and floodplain
517 deposition. The abandonment of the western Daga meander belt not much after 1,500
518 years ago, suggest that the Ayeyawady started to flow on a single preferential course
519 close to that time. Meander belt construction on the old and new course of the river,
520 leading to the formation of alluvial ridges, appears to be an efficient type of aggradation
521 on the upper delta plain before the river starts to bifurcate.

522

523 Near the coast, the quasi-contemporary beach ridge development on the Bogale
524 Promontory and Yangon River mouth suggest that the advanced position of the western
525 half of the delta was acquired early and maintained during progradation. Delta growth
526 since 6,300 years ago, with intermediate stages delineated by successive beach ridge sets,
527 suggest decreasing rates of advance of ~25 m/year until ~4,600 years ago and 8 to 10
528 m/year afterwards. The latter are still higher than the average progradation value of 3.4
529 m/year calculated by *Hedley et al. (2010)* for the last century or so. Furthermore, the
530 recent progradation occurred primarily on the coast adjacent to both sides of the Yangon
531 River, while the shoreline of the rest of the delta has been largely immobile.

532

533 It is important to note that, like the Ayeyawady, many large river deltas developing under
534 the Asian monsoon regime, such as Mekong (*Ta et al., 2002*), Red River (*Tanabe et al.,*
535 *2003*), or Godavari (*Cui et al., 2017*) started to form wave-built beach ridges between
536 5000 and 4000 years ago changing from river-dominated morphologies to show stronger
537 wave-influenced characteristics. Given that these deltas were at various stages of advance
538 from within their incised valleys onto the shelf it is more likely that their morphological
539 evolution was climatically driven rather than controlled by local factors as previously
540 proposed. As the late Holocene monsoon aridification started at that time (*Ponton et al.,*
541 *2012*), fluvial discharge variability at centennial timescales increased, setting the stage
542 for periodic wave-dominance of deltaic coasts during more arid intervals.

543

544 Our re-evaluation of the shelf morphology in the context of the new data onland reveals
545 important information for understanding the peculiar, irregular growth of the Ayeyawady
546 delta with its western half from Cape Maw Deng to the Bogale Promontory well
547 advanced into the Andaman Sea in comparison to its eastern half. First, the shelf DEM
548 suggests that the western Ayeyawady delta continues offshore into a shallow, shore-
549 attached cliniform, which is not completely unexpected given the relatively low tidal
550 range of 2–3 m (e.g., *Goodbred and Saito, 2012*) and the perennial loss of sediment
551 advected to the Gulf of Mottama (*Ramaswamy and Rao, 2014*). The Nd and Sr
552 fingerprint of the river sediment is almost identical to the beach ridge at Bogale
553 indicating that essentially no sediment from the Gulf of Mottama bearing the radiogenic
554 imprint of Sittaung (see above) and especially Thanlwin (*Damodararao et al., 2016*) is

555 feeding this part of the coast. The shore-attached sandy clinoform tapers off after 40 mbsl
556 (Fig. 2b). In contrast, the Gulf of Mottama exhibits a mid-shelf mud clinoform with the
557 roll-over at 40 m and toe depth of 80–90 m. The internal architecture of this distinctive
558 feature was imaged previously (*Ramaswamy and Rao, 2014*) showing seismic
559 characteristics typical of a clinoform topset and foreset. High rates of
560 progradation/aggradation for the Mottama clinoform have been suggested previously but
561 a core collected on its lower foreset has an average sedimentation rate of ~1 cm/year
562 since ~1450 AD (*Ota et al., 2017*), which is one order of magnitude less than proposed
563 before (*Chhibber, 1934; Rodolfo, 1975*). Given the depressed character of the Mottama
564 shelf indicated by the shelf edge position 40 to 70 meter lower than in front of the
565 western Ayeyawady delta perhaps, it is not surprising that infilling of this region is still
566 ongoing. What is surprising instead is why and how the Ayeyawady River built its delta
567 on the eastern raised shelf block rather than in advancing preferentially into the Gulf of
568 Mottama, defying theoretical and modeling expectations of a more advanced deltaic coast
569 toward the subsided block (e.g., *Liang et al., 2016*). The key to this problem appears to be
570 again suggested by the shelf morphology.

571
572 The distinctive transition between clinoforms exhibiting a wide elongated channel and
573 what appears to be an attached sediment drift-like feature suggests intense current activity
574 at the common boundary between the two clinoforms. Indeed tidal modeling suggests
575 that a tidal shear front (e.g., *Wang et al., 2017*) may be present in this region that shows a
576 drastic change from weak and more isotropic tidal currents west of Bogale Promontory to
577 highly oriented strong currents in the Gulf of Mottama (*Rizal et al., 2012*). Such a shear
578 front would explain both the unusual channel-drift couplet, but also the fact the
579 Ayeyawady was able to build its delta west of the gulf. If the tidal shear front has been a
580 long-lived feature of the shelf circulation it probably acted as a littoral energy fence
581 (*sensu Swift and Thorne, 1992*) trapping a significant part of the Ayeyawady coarser
582 sediment on the raised western shelf block. However, such an energy fence may be
583 broken by prevailing westerly currents during the summer monsoon when water and
584 sediment discharge peaks from the Ayeyawady to provide suspended sediment to the
585 Mottama clinoform. Given the depressed character of the Mottama shelf block, the front
586 must have existed since the beginning of the deglacial transgression of the northern
587 Andaman shelf. Industrial seismic reflection profiles imaged a region of strike-slip
588 extension in the Gulf of Mottama expressed as horsetail extensional splays linked to the
589 Sagaing Fault system (*Morley, 2017*) that can explain the height differential between the
590 western and eastern shelves. Furthermore, the shear front must have gradually intensified
591 through positive feedback with the morphology as the shore-attached clinoform west of it
592 grew larger. In contrast, the amplified tidal currents in the Gulf of Mottama efficiently
593 redistributed the significantly larger amount of Ayeyawady sediments that escaped
594 beyond the energy fence together with sediments from Sittaung and Thanlwin to form the

595 midshelf clinoform there. The offshore-directed tidal pumping leading to the formation of
596 the Mottama clinoform is reminiscent of the situation on the eastern Indus shelf where
597 strong tidal currents from the Gulf of Kutch built a mid-shelf clinoform with Indus
598 sediments escaping eastward (*Giosan et al., 2006*). Such clinoforms, which are of purely
599 tidal origin, and do not front a subaerial deltaic counterpart *per se* may have been more
600 common in sediment-rich macrotidal environments during faster transgressive conditions
601 in the past.

602

603 Conclusions

604

605 The Ayeyawady delta in Myanmar is the last realization in a long series of depocenters
606 that gradually moved southward within the tectonically dynamic intra-mountainous
607 landscape extending from the Central Myanmar Basin in the north to the northern
608 Andaman Sea in the south (Figs. 1 and 2). The delta appears to be vertically stable within
609 the incised valley dug by the Ayeyawady River during the last lowstand (Fig. 3). The
610 Pleistocene valley was flooded at least 80 km inland from the present coast during the
611 deglacial sea level rise. Holocene progradation into this paleo-Ayeyawady Bay proceeded
612 in the form of a fluvial- and tide-dominated delta until late Holocene wave action began
613 to build isolated and clustered beach ridges at the contemporaneous coasts (Fig. 2).
614 However, beach ridges are rather rare and underdeveloped, testifying to the enormous
615 sediment load discharged by the Ayeyawady and tidal dispersal and reworking. Ridge
616 construction during the late Holocene, similar to other several deltas across the Indian
617 monsoon domain, suggests a possible climatic control on delta morphodynamics through
618 variability in discharge, changes in wave climate, or both.

619

620 The landscape near the delta apex exhibits active and fossil late Holocene meander belts
621 that terminate in the mid-delta where the discharge is split to lower order distributary
622 channels (Fig. 2). The meander belts stand as alluvial ridges above the floodplain along
623 the active river course, as well as its antecedent paleo-course documenting the
624 Ayeyawady's avulsive character. Construction of a more advanced coast in the western
625 half of the delta could be seen as a quasi-independent region, the Pathein lobe (Fig. 5),
626 which was probably favored by the more western location of the early course of the river
627 (but see below). The eastern region of the delta (the Yangon lobe) is offset inland (Fig. 5)
628 and exhibits a more wave-dominated morphology, largely built with Ayeyawady-derived
629 sediment escaping alongshore. Further east, the Yangon lobe merges with the mudflats
630 fringing the Sittaung estuary (Fig. 5). Despite its large sediment load the Thanlwin River
631 has only built a bayhead delta, barely prograding outside its incised valley, probably due
632 to extreme macrotidal conditions at its mouth (Fig. 5). However, its sediment contributed
633 instead to deposition on the shelf, as did most of the load from both Ayeyawady and
634 Sittaung.

635

636 Correlation of the delta morphological and stratigraphic architecture information onland
637 to the shelf bathymetry and hydrodynamics, as well as its tectonic and sedimentary
638 characteristics, provides insight on the peculiar growth style of the Ayeyawady delta
639 (Figs. 2–5). The offset between the western Patheingyi lobe and the eastern deltaic coast
640 appears to be driven by tectonic-hydrodynamic feedbacks as the extensionally lowered
641 shelf block of the Gulf of Mottama amplifies tidal currents relative to the eastern part of
642 the shelf. This situation probably activates a perennial shear front between the two
643 regions that acts as a leaky energy fence. Just as importantly, the strong currents in the
644 Gulf of Mottama act as an offshore-directed tidal pump that help build a deep, mixed-
645 source mid-shelf clinoform, the Ayeyawady-Sittaung-Thanlwin subaqueous delta, into
646 the Mottama shelf depression.

647

648 Our study takes a first look at the evolution of the Holocene Ayeyawady delta to provide
649 a basis for more detailed work and context to present and future management plans for
650 this ecologically and economically important, but vulnerable region. A first conclusion
651 for the future of the region comes by comparing the Ayeyawady to other deltas across the
652 world. Uniquely for deltas of its size the Ayeyawady delta has not suffered a sediment
653 deficit from damming, yet it has been barely growing. The reason is the highly energetic
654 tidal, wind and wave regime of the northern Andaman Sea that export most sediments
655 offshore despite the large load of the river as envisioned by *Ramswamy et al., (2004)* and
656 *Hedley et al. (2010)*. In addition to their effects upstream (*Brakenridge et al., 2017*), the
657 expected sediment deficit after dams are constructed on the river and tributaries may
658 significantly impact the delta fragile sedimentary equilibrium (*Giosan et al., 2014*)
659 rendering it more vulnerable to the accelerating sea level rise (*Syvitski et al., 2009*) or
660 changes in frequency and intensity of cyclones hitting the coast (*Darby et al., 2016*)
661 compounding with increased subsidence linked to the rapid development of the region
662 (e.g., *Van der Horst, 2017*).

663

664

665 Acknowledgments

666

667 This study was primarily supported by an Andrew W. Mellon Foundation Award for
668 Innovative Research from the Woods Hole Oceanographic Institution to L. Giosan.
669 Additional funds were provided by the Charles T. McCord Chair in Petroleum Geology
670 to P. Clift. We thank Myanmar authorities for project permissions as well as leaders and
671 residents of villages that we visited in the Ayeyawady delta for hospitality and help. We
672 also thank V. Ramaswamy (NIO, Goa) for providing inspiration with his previous
673 Andaman Sea work and for help with initial contacts in Myanmar. N. Khonde gratefully
674 acknowledges the SERB Indo-US Postdoctoral Fellowship sponsored by SERB-IUSSTF
675 for research work at Woods Hole Oceanographic Institution, USA.

676

677 References

678

- 679 Adas, M.: The Burma Delta: Economic Development and Social Change on an Asian
680 Rice Frontier, 1852–1941, New Perspectives in SE Asian Studies, Univ. of Wisconsin
681 Press, 2011.
- 682 Allen, R., Najman, Y., Carter, A., Barfod, D., Bickle, M.J., Chapman, H.J., Garzanti, E.,
683 Vezzoli, G., Andò, S. and Parrish, R.R.: Provenance of the Tertiary sedimentary rocks
684 of the Indo-Burman Ranges, Burma (Myanmar): Burman arc or Himalayan-derived?,
685 *Journal of the Geological Society*, 165(6), 1045-1057, 2008.
- 686 Bender, F.: *Geology of Burma*, Gebrüder Borntraeger, Berlin, 1983.
- 687 Brakenridge, G.R., Syvitski, J.P.M., Nieburh, E., Overeem, I., Higgins, S.A., Kettner, A.
688 J. and Prades, L.: Design with nature: causation and avoidance of catastrophic
689 flooding, Myanmar. *Earth-Science Rev.* 165, 81–109, 2017.
- 690 British Admiralty: Bay of Bengal. East Coast. Sheet III. Coronge Island to White Point,
691 including the Gulf of Martaban, 1935.
- 692 Bronk Ramsey, C.: Bayesian analysis of radiocarbon dates. *Radiocarbon*, 51(1), 337-360,
693 2009.
- 694 Chhibber H. L.: *The Geology of Burma*. Macmillan, London, 1934.
- 695 Colarossi, D., Duller, G.A.T., Roberts, H.M., Tooth, S. and Lyons, R.: Comparison of
696 paired quartz OSL and feldspar post-IR IRSL dose distributions in poorly bleached
697 fluvial sediments from South Africa, *Quaternary Geochronology*, 30, 233-238, 2015
- 698 Colin, C., Turpin, L., Bertraux, J., Desprairies, A. and Kissel, C.: Erosional history of the
699 Himalayan and Burman ranges during the last two glacial–interglacial cycles, *Earth
700 and Planetary Science Letters*, 171, 647–660,1999.
- 701 Croudace, I.W. and Rothwell, R.G.: *Micro-XRF Studies of Sediment Cores,*
702 *Developments in Paleoenvironmental Research*, 17, Springer, 2015.
- 703 Croudace, I.W., Rindby, A. and Rothwell, R.G. ITRAX: description and evaluation of a
704 new X-ray core scanner. In *New Techniques in Sediment Core Analysis* (ed.
705 Rothwell, R. G.), *Geol. Soc. Lond. Spec. Publ.* 267, 51–63, 2006.
- 706 Cui, M., Wang, Z., Nageshwara Rao, K., Sangode, S.J., Saito, Y., Chen, T., Kulkarni
707 Y.R., Ganga Kumar, K.Ch., and Demudu, V.: A mid-to-late Holocene record of
708 vegetation decline and erosion triggered by monsoon weakening and human
709 adaptations in the south–east Indian Peninsula; *The Holocene*, 0959683617715694,
710 2017.
- 711 Curray, J.R., Moore, D.G., Lawver, L.A., Emmel, F.J., and Raitt, R.W.: Tectonics of the
712 Andaman Sea and Myanmar, in Watkins, J., et al., eds., *Geological and Geophysical
713 Investigations of Continental Margins: American Association of Petroleum
714 Geologists Memoir* 29, 189–198, 1979.
- 715 Curray, J.R.: Tectonics of the Andaman Sea region: *Journal of Asian Earth Sciences*, 25,
716 187–232, 2005.
- 717 D’Arrigo, R. and Ummenhofer, C.C.: The climate of Myanmar: evidence for effects of
718 the Pacific Decadal Oscillation, *Int. J. Climatol.*, 35, 634–640, doi:10.1002/joc.3995,
719 2014.
- 720 Damodararao K., Singh S.K, Rai V.K., Ramaswamy, V. and Rao, P.S.: Lithology,
721 Monsoon and Sea-Surface Current Control on Provenance, Dispersal and Deposition
722 of Sediments over the Andaman Continental Shelf, *Front. Mar.Sci.*, 3, 118, 2016.

723 Darby, S.E., Hackney, C.R., Leyland, J., Kumm, M., Lauri, H., Parsons, D.R., Best,
724 J.L., Nicholas, A.P. and Aalto, R.: Fluvial sediment supply to a mega-delta reduced
725 by shifting tropical-cyclone activity, *Nature* 539, 276-279, 2016.

726 Duller, G.A.T.: Distinguishing quartz and feldspar in single grain luminescence
727 measurements, *Radiation Measurements* 37, 161–165, 2003.

728 Farr, T.G., Rosen, P.A., Caro, E., Crippen, R., Duren, R., Hensley, S., Kobrick, M.,
729 Paller, M., Rodriguez, E., Roth, L. and Seal, D.: The Shuttle Radar Topography
730 Mission, *Rev Geophys* 45, 2007.

731 Fritz, H.M., Blount, C.D., Thwin, S., Thu, M.K. and Chan, N.: Cyclone Nargis storm
732 surge in Myanmar, *Nature Geoscience*, 2, 448-449, 2009.

733 Furuichi, T., Win, Z., and Wasson, R.J.: Discharge and suspended sediment transport in
734 the Ayeyarwady River, Myanmar: centennial and decadal changes. *Hydrol. Process.*
735 23, 1631–1641, 2009.

736 Garzanti, E., Wang, J.G., Vezzoli, G. and Limonta, M.: Tracing provenance and sediment
737 fluxes in the Irrawaddy River basin (Myanmar). *Chemical Geology*, 440, 73–90,
738 2016.

739 Gebregiorgis, D., Hathorne, E. C., Sijinkumar, A. V., Nagender Nath, B., Nürnberg, D.
740 and Frank, M.: South Asian summer monsoon variability during the last ~54 kyrs
741 inferred from surface water salinity and river run off proxies, *Quaternary Science*
742 *Reviews* 138, 6-15, 2016.

743 Giosan, L., Constantinescu, S., Clift, P.D., Tabrez, A. R., Danish, M. and Inam, A.:
744 Recent morphodynamics of the Indus delta shore and shelf, *Continental Shelf*
745 *Research*, 26,1668-1684, 2006.

746 Giosan, L., Ponton, C., Usman, M., Blusztajn, J., Fuller, D., Galy, V., Haghipour, N.,
747 Johnson, J., McIntyre, C., Wacker, L. and Eglinton, T.: Massive Erosion in
748 Monsoonal Central India Linked to Late Holocene Landcover Degradation, *Earth*
749 *Surface Dynamics*, 5, 781, 2017.

750 Giosan, L., Syvitski, J. P. M., Constantinescu, S., and Day, J.: Protect the World's Deltas,
751 *Nature*, 516, 31-33, 2014.

752 Godfrey-Smith, D.L., Huntley, D. J. and Chen, W.H.: Optically dating studies of quartz
753 and feldspar sediment extracts. *Quaternary Science Reviews* 7, 373–380. 1988

754 Goodbred S.L. and Saito, Y.: Tide dominated deltas. In *Principles of Tidal*
755 *Sedimentology*, ed. RA Davis Jr, RW Dalrymple, 129–49. London: Springer, 2012.

756 Gordon, R.: Hydraulic work in the Irawadi Delta, *Proc. Inst. Civ. Eng.* 113, 276–313,
757 1893.

758 Hedley, P.J., Bird, M.I. and Robinson, R.A.J.: Evolution of the Irrawaddy delta region
759 since 1850, *Geogr. J.*, 176, 138–149, 2010.

760 Hoitink, A.J.F., Wang, Z.B., Vermeulen, B., Huisman, Y. and Kästner, K.: Tidal
761 controls on river delta morphology, *Nature Geoscience*, 10, 637-645, 2017.

762 Kars, R.H., Reimann, T., Ankjaergaard, C. and Wallinga, J.: Bleaching of the post-IR
763 IRSL signal: new insights for feldspar luminescence dating, *Boreas*, 43, 780–791.
764 2014

765 Kravtsova, V.I., Mikhailov, V.N. and Kidyayeva, V.M.: Hydrological regime,
766 morphological features and natural territorial complexes of the Irrawaddy River Delta
767 (Myanmar), *Vodn. Resur.*, 36, 259–276, 2009.

768 Lee, H.Y., Chung, S.L. and Yang, H.M.: Late Cenozoic volcanism in central Myanmar:
769 Geochemical characteristics and geodynamic significance, *Lithos* 245, 174-190, 2016
770 Liang, M., Kim, W. and Passalacqua, P.: How much subsidence is enough to change the
771 morphology of river deltas?, *Geophysical Research Letters*, 43, 2016.
772 Licht, A., Reisberg, L., France-Lanord, C., Naing Soe, A., and Jaeger, J.J.: Cenozoic
773 evolution of the central Myanmar drainage system: insights from sediment
774 provenance in the Minbu Sub-Basin, *Basin Research*, 28, 237-251, 2016.
775 Liu, C.Z., Chung, S.L., Wu, F.Y., Zhang, C., Xu, Y., Wang, J.G., Chen, Y., and Guo, S.:
776 Tethyan suturing in Southeast Asia: Zircon U-Pb and Hf-O isotopic constraints from
777 Myanmar ophiolites. *Geology*, 44, 311-314. 2016.
778 Madsen, A.T., Buylaert, J.-P. and Murray, A.S.. Luminescence dating of young coastal
779 deposits from New Zealand using feldspar. *Geochronometria* 38, 378-390, 2011.
780 Matamin, A.R., Ahmad, F., Mamat, M., Abdullah, K. and Harun, S.: Remote sensing of
781 suspended sediment over Gulf of Martaban, *Ekologia*, 34, 54-64, 2015.
782 McHugh, M.G.C., Gurung, D., Giosan, L., Ryan, W.B.F., Mart, Y., Sancar, U., Burckle,
783 L., and Çagatay, M.N.: The last reconnection of the Marmara Sea (Turkey) to the
784 World Ocean: A paleoceanographic and paleoclimatic perspective, *Marine Geology*,
785 255, 2008.
786 Milliman, J.D. and Farnsworth, K.L.: *River Discharge to the Coastal Ocean: A Global
787 Synthesis*, Cambridge Univ. Press, Cambridge, 2010.
788 Moore E.H.: *Early Landscapes of Myanmar*, River Books, Bangkok , pp., 272, 2006.
789 Morley, C.K.: Cenozoic rifting, passive margin development and strike-slip faulting in
790 the Andaman Sea: a discussion of established v. new tectonic models. In:
791 Bandopadhyay, P.C. & Carter, A. (eds) *The Andaman–Nicobar Accretionary Ridge:
792 Geology, Tectonics and Hazards*. Geological Society, London, *Memoirs*, 47, 27–50,
793 2007.
794 Murray, A.S. and Wintle, A.G.: Luminescence dating of quartz using an improved single-
795 aliquot regenerative-dose protocol. *Radiation Measurement* 32, 57–73, 2000.
796 Murray, A.S., Marten, R., Johnston, A. and Martin, P.: Analysis for naturally occurring
797 radionuclides at environmental concentrations by gamma spectrometry. *Journal of
798 Radioanalytical and Nuclear Chemistry*, 115, 263–288, 1987.
799 Murray, A.S., Thomsen, K.J., Masuda, N., Buylaert, J.-P. & Jain, M.: Identifying well-
800 bleached quartz using the different bleaching rates of quartz and feldspar
801 luminescence signals, *Radiation Measurements*, 47, 688–695, 2012.
802 Ota, Y., Kawahata, H., Murayama, M., Inoue, M., Yokoyama, Y., Miyairi, Y., Aung, T.,
803 Hossain, H.M.Z., Suzuki, A., Kitamura, A., and Moe, K.T.: Effects of intensification
804 of the Indian Summer Monsoon on northern Andaman Sea sediments during the past
805 700 years, *J. Quat. Sci.*, 32, 528–539, 2017.
806 Ponton, C., Giosan, L., Eglinton, T. ., Fuller, D.J., Johnson, E., Kumar, P. and Collet,
807 T.S.: Holocene Aridification of India, *Geophysical Research Letters*, 39, p. L03704,
808 2012.
809 Racey, A. and Ridd, M.F.: *Petroleum Geology of Myanmar*. Geological Society of
810 London, 2015.
811 Ramaswamy V., Rao P.S., Rao K.H., Thwin, S., Rao, Srinivasa N. and Raiker, V.: Tidal
812 influence on suspended sediment distribution and dispersal in the northern Andaman
813 Sea and Gulf of Martaban, *Marine Geology*, 208, 33–42, 2004.

814 Ramaswamy, V., and Rao, P.S.: The Myanmar continental shelf. In F. L. Chiocci & A. R.
815 Chivas (Eds.), *Continental Shelves of the World: Their Evolution During the Last*
816 *Glacio-Eustatic Cycle* (pp. 231-240). Bath, UK: Geological Society of London, 2014.
817 Rao, P.S., Ramaswamy, V. and Thwin, S.: Sediment texture, distribution and transport on
818 the Ayeyarwady continental shelf, *Andaman Sea, Mar. Geol.*, 216, 239–247, 2005.
819 Reimer P.J., Bard, E., Bayliss, A., Beck, J.W., Blackwell, P.G., Bronk, Ramsey C., Buck,
820 C.E., Edwards, R.L., Friedrich, M., Grootes, P.M., Guilderson, T.P., Hafliðason, H.,
821 Hajdas, I., Hatté, C., Heaton, T.J., Hoffman, D.L., Hogg, A.G., Hughen, K.A., Kaiser,
822 K.F., Kromer, B., Manning, S.W., Niu, M., Reimer, R.W., Richards, D.A., Scott, M.,
823 Southon, J.R., Staff, R.A., Turney, C.S.M., van der Plicht, J.: *IntCal13 and Marine13*
824 *radiocarbon age calibration curves 0–50,000 years cal BP, Radiocarbon* 55: 1869–
825 1887, 2013.
826 Rémillard, A.M., St-Onge, G., Bernatchez, P., Hétu, B., Buylaert, J.-P., Murray, A.S.,
827 and Vigneault, B.: Chronology and stratigraphy of the Magdalen Islands archipelago
828 from the last glaciation to the early Holocene: new insights into the glacial and sea-
829 level history of eastern Canada, *Boreas*, 45, 604-628, 2016.
830 Rizal, S., Damm, P., Wahid, M.A., Sundermann, J., Ilhamsyah, Y. and Iskandar T.:
831 General circulation in the Malacca Strait and Andaman Sea: A numerical model
832 study. *American Journal of Environmental Sciences*, 8, 479-488, 2012.
833 Robinson, R.A.J., Bird, M.I., Oo, N.W., Hoey, T.B., Aye, M.M., Higgitt, D.L., Swe, A.,
834 Tun, T. and Win, S.L.: The Irrawaddy river sediment flux to the Indian Ocean: the
835 original nineteenth-century data revisited, *Journal of Geology*, 115, 629-640, 2007.
836 Rodolfo, K. S.: Bathymetry and marine geology of the Andaman Basin, and tectonic
837 implications for Southeast Asia, *GSA Bulletin*, 80, 1203–1230, 1969a.
838 Rodolfo, K. S.: Sediments of the Andaman Basin, Northeastern Indian Ocean, *Mar.*
839 *Geol.*, 7, 371– 402, 1969b.
840 Rodolfo, K.S.: The Irrawaddy Delta: Tertiary setting and modern offshore sedimentation.
841 In *Deltas: Models for Exploration*, Broussard ML (ed.). Houston Geological Society:
842 Houston, 329–348, 1975.
843 Scher H.D. and Delaney, M.L.: Braking the glass ceiling for high resolution Nd records
844 in early Cenozoic paleoceanography, *Chemical Geology*, 269, 269-329, 2010.
845 Seekins, D.M.: State, society and natural disaster: cyclone Nargis in Myanmar (Burma),
846 *Asian Journal of Social Science*, 37, 717-37, 2009.
847 Shi, W. and Wang, M.: Three-dimensional observations from MODIS and CALIPSO for
848 ocean responses to cyclone Nargis in the Gulf of Martaban, *Geophysical Research*
849 *Letters*, 35, L21603, 2008.
850 Stamp, D.L.: The Irrawaddy River. *Geogr. J.*, 5, 329–352, 1940.
851 Swift, D.J.P. and Thorne, J.A.: Sedimentation on Continental Margins, I: A General
852 Model for Shelf Sedimentation, in *Shelf Sand and Sandstone Bodies: Geometry,*
853 *Facies and Sequence Stratigraphy* (eds D. J. P. Swift, G. F. Oertel, R. W. Tillman and
854 J. A. Thorne), Blackwell Publishing Ltd., Oxford, UK, 1992.
855 Syvitski, J.P., Kettner, A.J., Overeem, I., Hutton, E.W., Hannon, M.T., Brakenridge,
856 G.R., Day, J., Vörösmarty, C., Saito, Y., Giosan, L. and Nicholls, R.J., Sinking deltas
857 due to human activities, *Nature Geoscience*, 2, 681-686, 2009.
858 Ta, T.K.O., Nguyen, V.L., Tateishi, M., Kobayashi, I., Saito, Y. and Nakamura, T.:
859 Sediment facies and Late Holocene progradation of the Mekong River Delta in Bentre

860 Province, southern Vietnam: an example of evolution from a tide-dominated to a tide-
861 and wave-dominated delta. *Sedimentary Geology*, 152, 313-325, 2002.

862 Taft, L. and Evers, M.: A review of current and possible future human-water dynamics in
863 Myanmar's river basins, *Hydrological Earth System Science*, 20, 4913-4928, 2016.

864 Tanabe, S., Hori, K., Saito, Y., Haruyama, S. and Kitamura, A.: Song Hong (Red River)
865 delta evolution related to millennium-scale Holocene sea-level changes, *Quaternary*
866 *Science Reviews*, 22, 2345-2361, 2003.

867 Thomsen, K., Murray, A.S., Jain, M. and Bøtter-Jensen, L.: Laboratory fading rates of
868 various luminescence signals from feldspar-rich sediment extracts, *Radiation*
869 *Measurements*, 43, 1474–1486, 2008.

870 Van der Horst, T.: Sinking Yangon: Detection of subsidence caused by groundwater
871 extraction using SAR interferometry and PSI time-series analysis for Sentinel-1 data.
872 MS Thesis, Delft University of Technology and the National University of Singapore,
873 <http://repository.tudelft.nl>, 2017.

874 Volker, A.: The deltaic area of the Irrawaddy river in Burma, in *Scientific problems of*
875 *the humid tropical zone deltas and their implications*, Proceedings of the Dacca
876 Symposium, UNESCO, 373–379, 1966.

877 Wang, N., Li, G., Qiao, L., Shi, J., Dong, P., Xu, J. and Ma, Y.: Long-term evolution in
878 the location, propagation, and magnitude of the tidal shear front off the Yellow River
879 Mouth, *Continental Shelf Research*, 137, 1-12, 2017.

880

881
882
883

Table 1. Results of AMS ¹⁴C dating of organic materials from drill cores IR1 (Kyonmangay) and IR2 (Ta Loke Htaw).

Location	Sample	Altitude (<i>m bsf</i>)	Type	Labcode	Latitude	Longitude	Age (<i>years BP</i>)	Error (<i>years BP</i>)	d13C (<i>per mil</i>)	Calibrated Age (<i>years</i>)*	Error (<i>years</i>)	Observations
Kyonmangay	IR1-9.60	-2.9	leaf fragment	OS-132754	16°26'15N	95°08'01"E	5,590	100	-28.65	6487	213	small
Kyonmangay	IR1-20.0	-13.3	leaf fragment	OS-132658	16°26'15N	95°08'01"E	7,300	40	-26.71	8166	80	
Kyonmangay	IR1-35.0	-28.3	mangrove wood piece	OS-133490	16°26'15N	95°08'01"E	8,300	40	-27.27	9352	148	
Kyonmangay	IR1-40.0	-33.3	carbonized wood piece	OS-132659	16°26'15N	95°08'01"E	9,100	35	-26.58	10351	88.5	
Ta Loke Htaw	IR2-19.0	-0.5	wood trunk piece	OS-133606	17°39'13"N	95°26'2"E	1,320	15	-28.04	1307	53.5	
Ta Loke Htaw	IR2-33.5	-15.0	carbonized wood piece	OS-135132	17°39'13"N	95°26'2"E	8,020	30	-27.7	8959	117.5	small

*Calendar ages are relative to year 2016

884
885

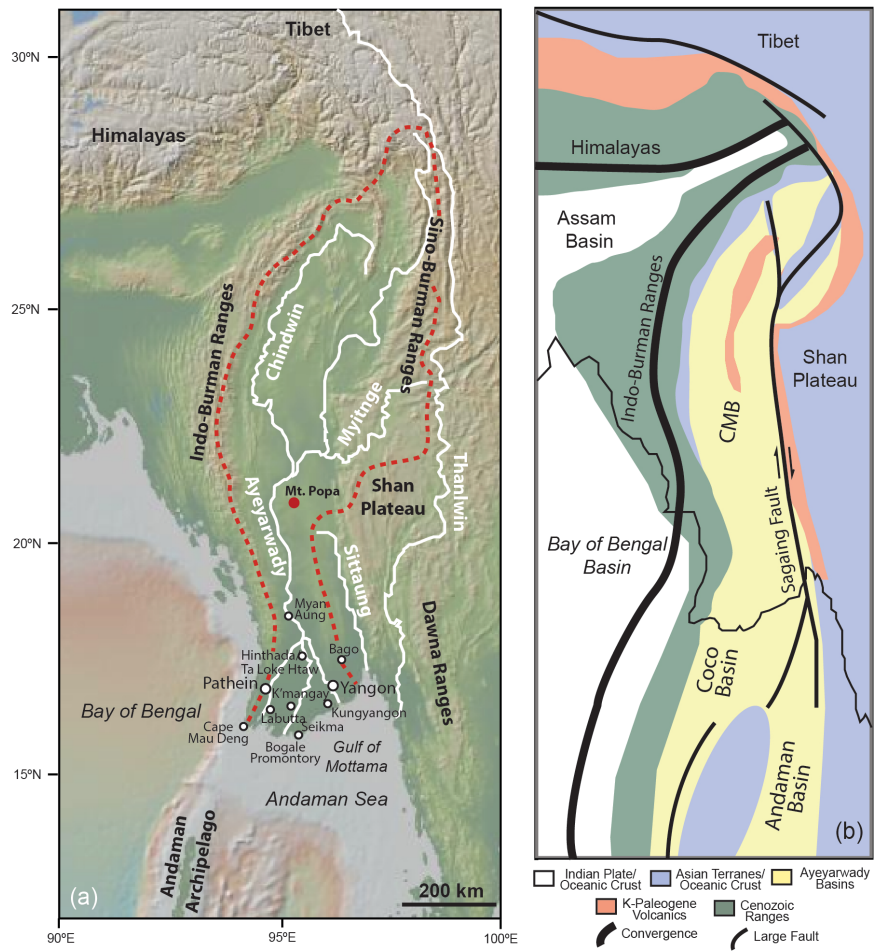
886 Table 2. Summary of the quartz and feldspar luminescence data. (n) denotes the number of aliquots contributing to dose (De). The
 887 saturated water content (w.c.) is given as the ratio of weight of water to dry sediment weight. Feldspar IR50 and pIRIR150 ages have
 888 not been corrected for any signal instability. Radionuclide concentrations used to derive quartz and feldspar dose rates are given in
 889 Table S1. Bleaching of quartz OSL signal is assessed by comparing the quartz ages with the IR50 and pIRIR150 ages. Uncertainties
 890 represent one standard error. Age uncertainties include random and systematic components. Quartz ages should be used for
 891 interpretation; feldspar ages are only used to investigate quartz OSL bleaching.

892
 893

Sample code	Site	Setting	Latitude / Longitude	Depth, cm	Quartz well-bleached?	Quartz Age , ka	pIRIR ₁₅₀ Age , ka	IR ₅₀ Age , ka	Quartz Dose , Gy (n)	pIRIR ₁₅₀ Dose , Gy	IR ₅₀ Dose , Gy (n)	Quartz Dose rate, Gy/ka	K-feldspar Dose rate, Gy/ka	w.c. %
17 72 01	18	fluvial levee	N 17 38 36.82 / E 95 18 33.64	95	probably	1.50 ± 0.23	6.64 ± 0.68	1.20 ± 0.23	3.28 ± 0.49 34	20.6 ± 1.9	3.73 ± 0.69 9	2.19 ± 0.10	3.10 ± 0.12	29
17 72 02	19	fluvial levee	N 17 36 13.5 / E 95 12 53.39	110	not certain	1.75 ± 0.32	15.2 ± 5.5	4.02 ± 1.85	4.14 ± 0.73 35	46 ± 16	12.0 ± 5.5 9	2.37 ± 0.10	2.99 ± 0.11	35
17 72 03	110	beach ridge	N 16 09 03.5 / E 94 43 57.3	92	probably	1.46 ± 0.22	2.35 ± 0.21	1.10 ± 0.07	2.97 ± 0.42 40	6.9 ± 0.5	3.25 ± 0.17 9	2.03 ± 0.09	2.95 ± 0.11	28
17 72 04	111	beach ridge	N 16 09.2578 / E 94 44.1843	90	confident	4.63 ± 0.47	4.73 ± 0.37	2.71 ± 0.17	10.1 ± 0.9 36	14.7 ± 1.0	8.42 ± 0.43 9	2.18 ± 0.09	3.10 ± 0.11	32
17 72 05	112	beach ridge	N 15 50 10.5 / E 95 29 51	100	probably	1.04 ± 0.09	1.94 ± 0.19	0.79 ± 0.05	2.64 ± 0.17 38	6.7 ± 0.6	2.72 ± 0.14 9	2.53 ± 0.13	3.45 ± 0.15	38
17 72 06	113	beach ridge	N 15 49.6494 / E 95 30.2095	132	probably	0.86 ± 0.07	1.86 ± 0.15	0.68 ± 0.04	1.58 ± 0.12 37	5.1 ± 0.4	1.88 ± 0.08 9	1.84 ± 0.07	2.75 ± 0.10	40
17 72 07	114	beach ridge	N 16 24 27.5 / E 96 02 20.2	115	probably	1.19 ± 0.11	1.43 ± 0.12	0.76 ± 0.04	2.64 ± 0.19 40	4.5 ± 0.3	2.38 ± 0.09 9	2.21 ± 0.10	3.13 ± 0.12	24

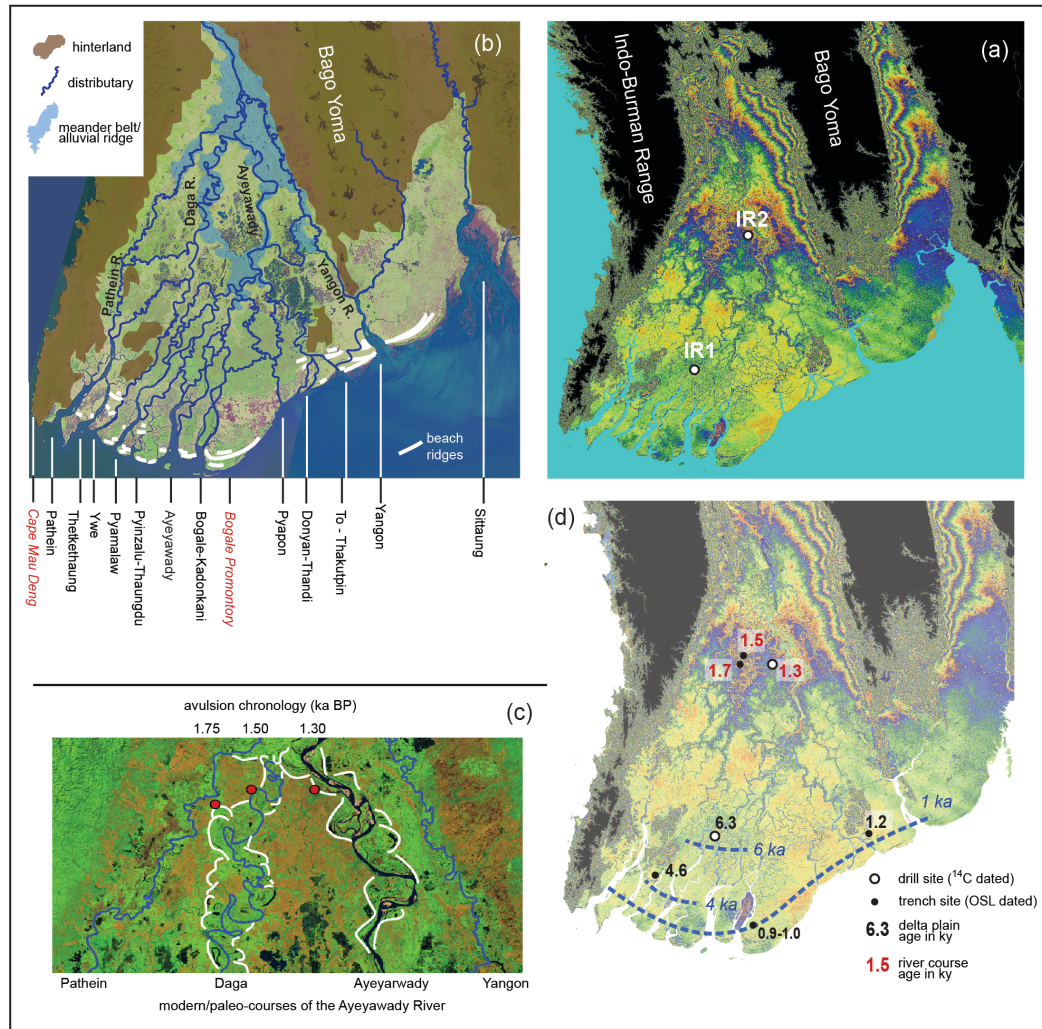
894

895 Fig. 1. (a) Physiography and (b) geology of the Ayeyarwady Basin and adjacent regions.
 896



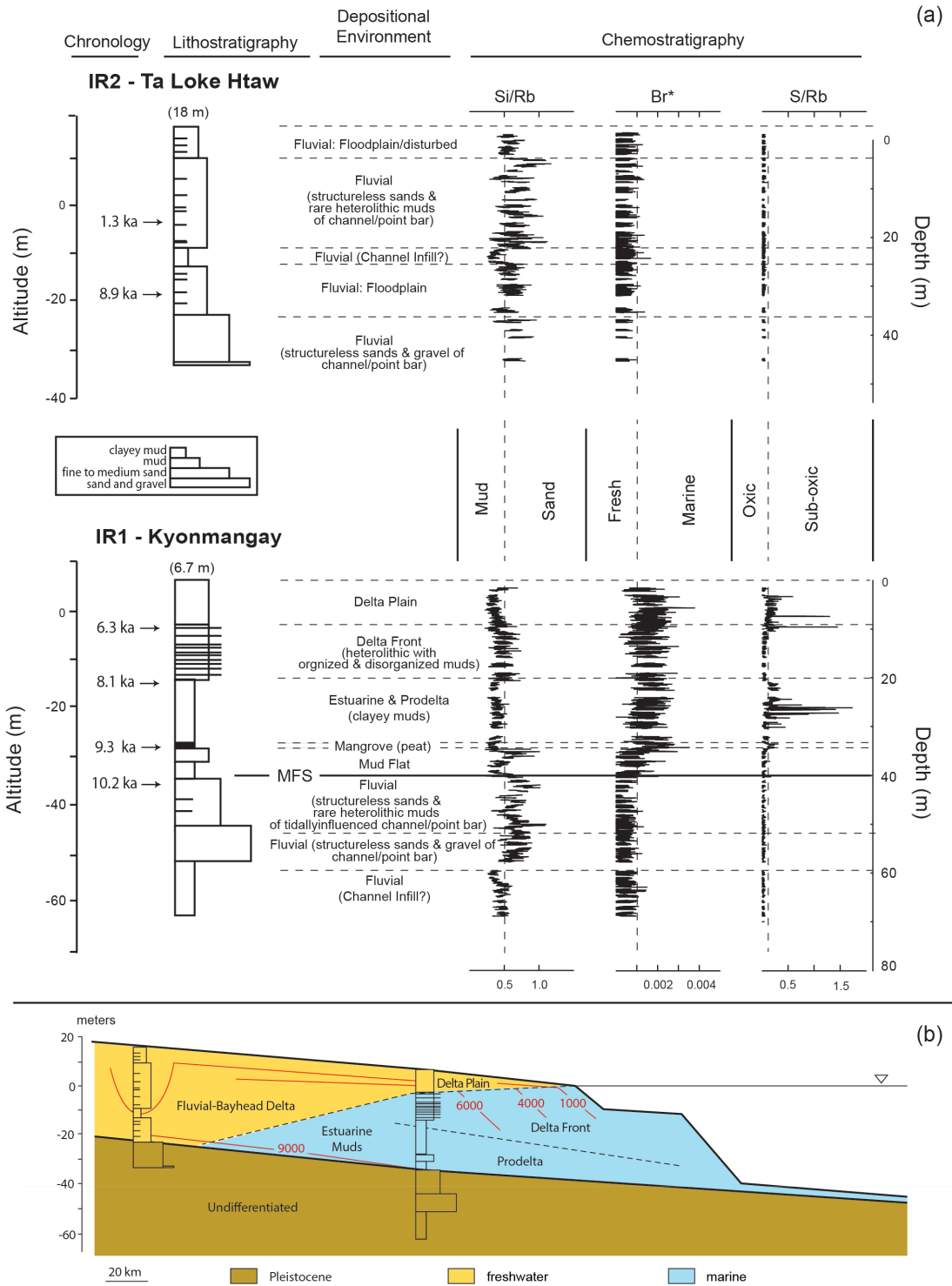
897
 898
 899

900 Fig. 2. (a) SRTM-derived DEM for the Ayeyawady delta region (pattern of colors repeats
 901 every 10 m to 300 m in height; higher landscape in black); (b) large scale features of the
 902 Ayeyawady delta region with identified river and distributary courses and mouths as well as
 903 beach ridges shown on an ASTER satellite photo ; (c) sample locations and chronology on the
 904 meander belts documenting the avulsion near the delta apex (meander belts as white lines
 905 delimited from ASTER and Google Earth images); (d) preliminary model of the Ayeyawady
 906 delta evolution with sampling locations and types with chronological information on the
 907 youngest fluvial deposits and beach ridges.
 908



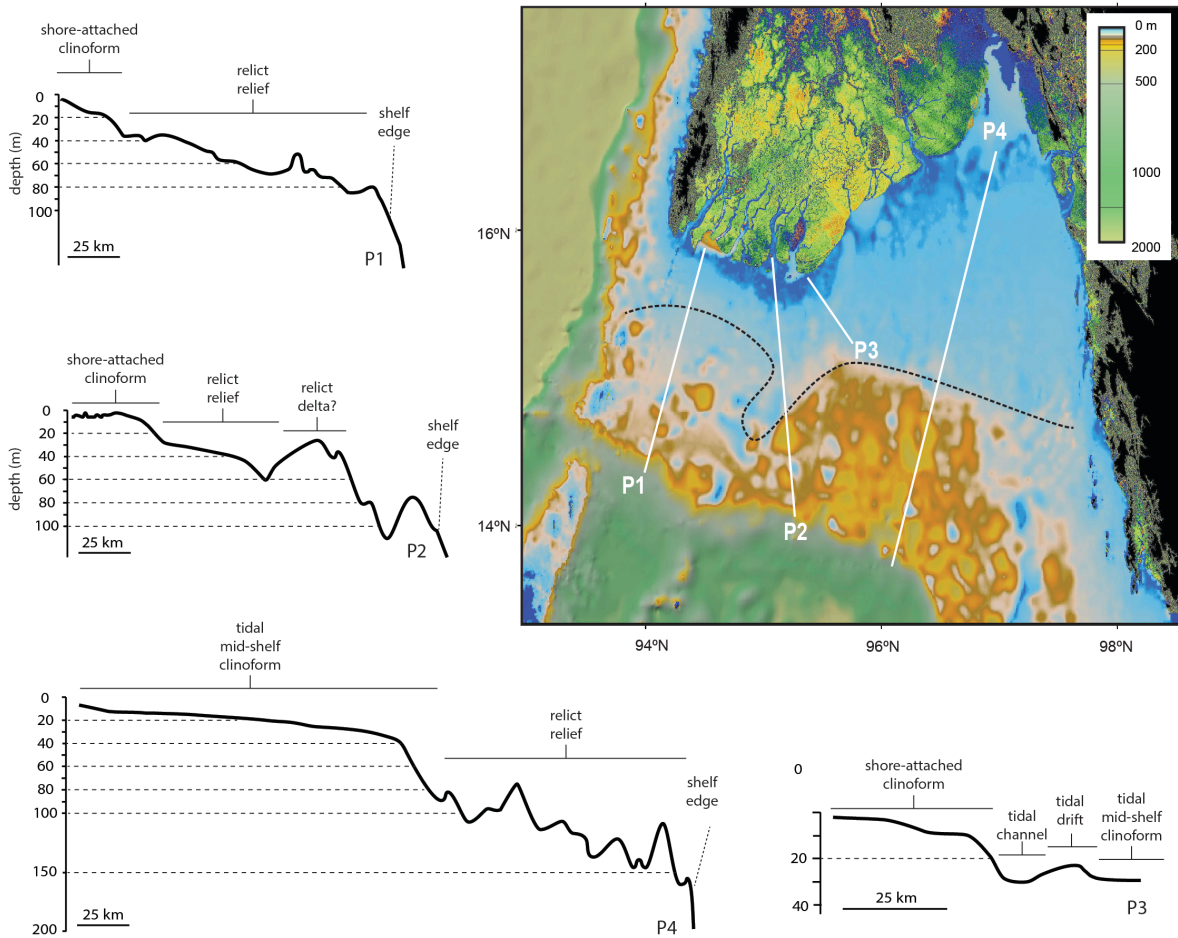
909
 910

911 Fig. 3. (a) Depositional environments interpreted from litho- and chemo-stratigraphy with
 912 radiocarbon chronology for drill cores in the Ayeyawady delta; (b) interpreted Ayeyawady
 913 delta stratigraphy and evolution along the Ayeyawady's main course.
 914



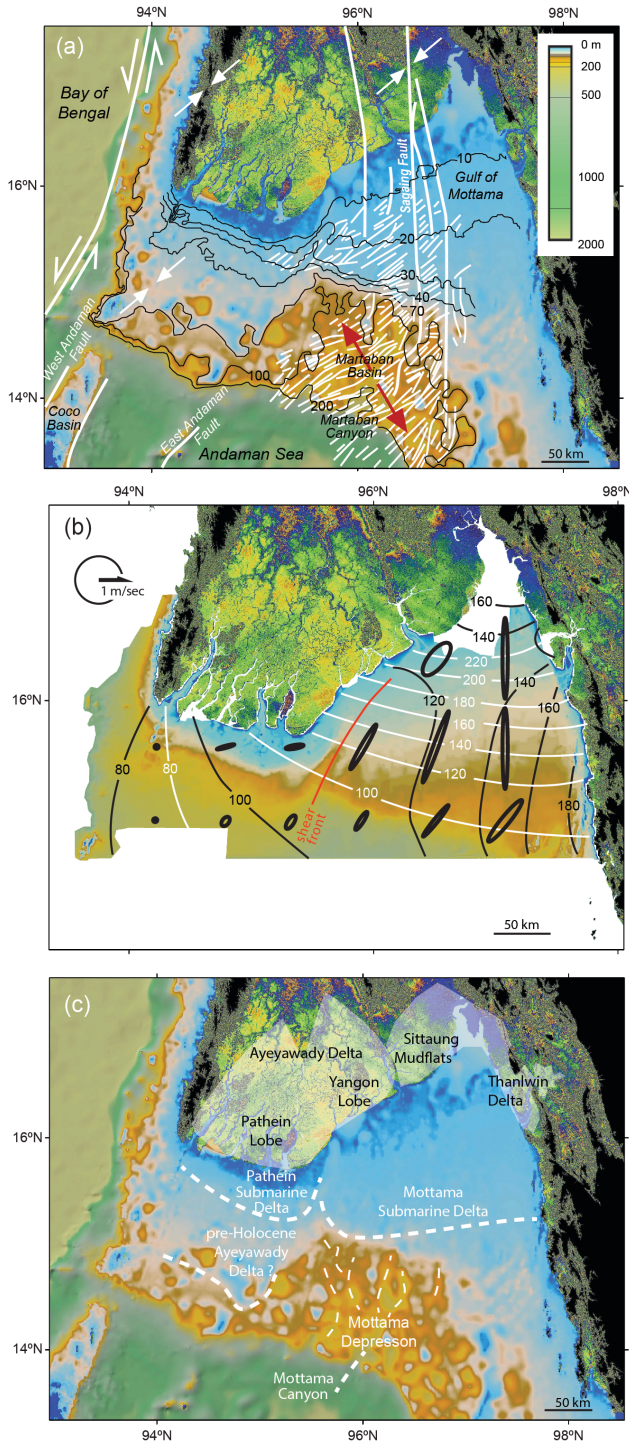
915
916

917 Fig. 4. Interpreted bathymetric profiles across the northern Andaman Sea shelf (bathymetric
 918 profiles identified on map). Dashed line on map indicates the approximate limit of consistent
 919 fine-grained sediment deposition on the shelf farthest from shore. The SRTM-derived DEM
 920 for the Ayeyawady delta region is shown onland.
 921



922
 923

924 Fig. 5. (a) Bathymetry of the northern Andaman Sea shelf and SRTM-derived DEM for the
 925 Ayeyawady delta region onland with regional faults and associated splay faults (Morley,
 926 2017); arrow pairs indicate regional compression (white) or extension (red); (b) tidal range
 927 lines (black), co-tidal lines (white) and tidal current magnitudes (ellipses) for the dominant
 928 M2 tide component (Rizal et al., 2012); (c) sketch the Ayeyawady delta plain evolution
 929 and associated subaqueous deltas.



930
 931